

Understanding Steady-State Free Precession: A Geometric Perspective

ROHAN DHARMAKUMAR, GRAHAM A. WRIGHT

Department of Medical Biophysics, Sunnybrook & Women's College Health Sciences Centre, Room S611, 2075 Bayview Avenue, University of Toronto, Toronto, Canada M4N 3M5

ABSTRACT: Steady-state free precession (SSFP) sequences are becoming more common in clinical and research studies. Though there have been mathematical treatments of SSFP signals, a simple and/or intuitive understanding of how such signals are established is lacking in the literature. In this work, the classical picture of a spin system is used to develop an analysis of the behavior of magnetization in phase space. This leads to a geometric description that demonstrates the essential features of SSFP signals. This analysis yields an intuitive understanding of SSFP signal formation and the intricate interactions between the choice of flip angle, pulse repetition time, relaxation effects, and phase-cycling patterns on the final SSFP signal. © 2005 Wiley Periodicals, Inc. Concepts Magn Reson Part A 26A: 1–10, 2005

KEY WORDS: SSFP; rapid MRI; spin manipulation; fixed points

AN OVERVIEW

The first report that nuclear ensembles can reach a steady state and precess about the static external magnetic field in the presence of repeated excitation by radiofrequency pulses was presented by Carr et al. (1) in 1958. However, only recently has this phenomenon been utilized extensively in imaging (2). The primary reason for this delay can be attributed to hardware limitations. For the desirable SSFP imaging method

(balanced SSFP), the imaging gradients must be fully refocused over small repetition periods (typically a few milliseconds), requiring rapidly switching magnetic field gradients that were not available until recently. With the required improvements in hardware, the SSFP technique has now become practical in clinical and research studies.

The distinguishing feature of the SSFP technique over many other MRI methods is that it offers significant improvements in spatial and temporal resolution with high tissue contrast (2). Though these benefits are useful in imaging any organ system, they are particularly relevant for cardiac imaging since the gating methods used to “freeze” the motion of the heart demand scan times in the order of several minutes (2). In addition to rapid acquisition of MR images with high signal-to-noise ratio (3, 4), such advances have also facilitated fast measurements of relaxation constants (5, 6) and in vivo maps of temperature (7)

Received 28 October 2004; revised 17 January 2005; accepted 17 January 2005

Correspondence to: Rohan Dharmakumar; E-mail: rohan@sten.sunnybrook.utoronto.ca

Concepts in Magnetic Resonance Part A, Vol. 26A(1) 1–10 (2005)

Published online in Wiley InterScience (www.interscience.wiley.com). DOI 10.1002/cmr.a.20033

© 2005 Wiley Periodicals, Inc.

and blood oxygen saturation (8). As SSFP methods are further refined to provide real-time anatomical and physiological information, it is important to reflect on how such signals are established.

Though a sound mathematical understanding of SSFP exists in the literature, there has been much less effort in exploring an intuitive understanding of how such signals are formed. In particular, a description of the interplay of the various imaging parameters determining the final steady-state signals is needed. There have been efforts to apply the elegant phase-graph method via the echo formation pathways (9). The primary purpose of this work is to put forth a more intuitive pedagogical model, from the viewpoint of classical dynamics, for understanding how SSFP signals are formed. In the past, geometrical descriptions of continuous-wave irradiation on spin ensembles have been explored (10). In this article, we consider the effect of short-pulsed irradiation on an ensemble of spins and how such pulses contribute to the establishment of a steady-state magnetization from a geometric perspective. In so doing, we develop a model for understanding the interplay between relaxation constants, flip angle, time between RF pulses (T_R), off-resonance, and phase-cycling patterns on the steady-state signal from a spin ensemble.

In the simplest terms, SSFP signals result from repeated application of RF pulses that tip the total

magnetization at a predetermined flip angle and time interval. In SSFP, after the application of every RF pulse, the magnetization evolves by recovering along the longitudinal direction and losing coherence in the transverse plane. The natural tendency of the spins' drive toward thermal equilibrium encountering a repeated perturbation by the RF pulses leads to the establishment of a steady-state MR signal. In this state, there is a dynamic equilibrium between the natural relaxation process and the magnetic perturbation, which leads to a free precession of the magnetization in the rotating frame. The analytic description of SSFP signals is reviewed in Appendix A.

THE GEOMETRY OF SSFP SIGNALS FROM A SPIN ENSEMBLE

Clearly, as shown in Appendix A, the closed-form Eqs. [16–21] describing the steady-state magnetization are complicated functions of α , β , T_1 , T_2 , and T_R . Given the interplay of these parameters in establishing steady-state magnetization, it is difficult to visualize how different steady-state signal values are established. In addition, no analytic equations have been derived for the transient behavior. The transient behavior is understood primarily from integrating the Bloch equations over each T_R . In this section, we develop a geometrical understanding of

List of Symbols:

\in ,	Element of;	$\mathcal{M}^+(n)$,	Magnetization of a spin ensemble with components
\subset ,	Subset of;	$(\mathcal{M}_x^+(n), \mathcal{M}_y^+(n), \mathcal{M}_z^+(n))$	immediately following the n^{th} RF pulse;
α ,	Flip angle;	\mathbf{M}_0 ,	Equilibrium magnetization or magnetic dipole moment per unit volume;
β ,	Phase rotation angle of a spin ensemble resulting from exposure to a spatially invariant magnetic field shift over a period of T_R ;	M_{xy} ,	Magnitude of the transverse component of magnetization;
β^* ,	Critical value of β given by Eq. [4];	M_z ,	Magnitude of the longitudinal component of magnetization;
γ ,	Gyromagnetic ratio of hydrogen nucleus (26.75×10^7 rad/s/T);	(M_x, M_y, M_z) ,	x , y , and z components of magnetization;
ΔB ,	Spatially invariant static magnetic field variation;	\mathbf{M}_{xy} ,	Transverse magnetization in phasor notation (i.e. $M_x \hat{\mathbf{i}} + M_y \hat{\mathbf{j}}$);
Ω ,	A subset of $[0, 2\pi]$ over which the magnitude of the SSFP signal is most slowly varying;	$M(T_E)$,	Magnitude of the SSFP signal at T_E ;
C ,	$(1 - E_1 \cos \alpha)(1 - E_2 \cos \beta) - E_2(E_1 - \cos \alpha)(E_2 - \cos \beta)$;	MR,	Magnetic resonance;
CPMG,	Carr-Purcell-Meiboom-Gill;	MRI,	Magnetic resonance imaging;
e ,	Eccentricity of the transverse magnetization locus given by Eq. [5];	n ,	Number of RF pulses;
E_1 ,	$\exp(-T_R/T_1)$;	NMR,	Nuclear magnetic resonance;
E_2 ,	$\exp(-T_R/T_2)$;	$p(\beta)$,	Probability density of random variable β ;
L_a ,	Length of major axis of transverse magnetization locus;	R_x ,	Rotation matrix about x axis;
L_b ,	Length of major axis of transverse magnetization locus;	R_z ,	Rotation matrix about z axis;
\mathcal{M}_0 ,	Equilibrium magnetization of a spin ensemble;	RF pulse,	Radio frequency pulse;
\mathcal{M} ,	Total magnetization of a spin ensemble with components $\mathcal{M}_x, \mathcal{M}_y, \mathcal{M}_z$;	S ,	A 3×3 diagonal matrix containing relaxation terms E_2 and E_1 ;
$\mathcal{M}^-(\infty)$,	Steady state ensemble magnetization immediately before the RF pulse with components $(\mathcal{M}_x^-(\infty), \mathcal{M}_y^-(\infty), \mathcal{M}_z^-(\infty)) = (\mathcal{M}_x^-, \mathcal{M}_y^-, \mathcal{M}_z^-)$;	SSFP,	Steady-state free precession;
$\mathcal{M}^+(\infty)$,	Steady state ensemble magnetization immediately following the RF pulse with components $(\mathcal{M}_x^+(\infty), \mathcal{M}_y^+(\infty), \mathcal{M}_z^+(\infty)) = (\mathcal{M}_x^+, \mathcal{M}_y^+, \mathcal{M}_z^+)$;	T_1 ,	Spin-lattice relaxation constant;
$\mathcal{M}^-(n)$,	Magnetization of a spin ensemble with components $(\mathcal{M}_x^-(n), \mathcal{M}_y^-(n), \mathcal{M}_z^-(n))$ immediately before the n^{th} RF pulse;	T_2 ,	Spin-spin relaxation constant;
		T_E ,	Echo time;
		T_R ,	Time between RF pulses

how the signal formation takes places by studying the evolution of the magnetization in phase space. In this context, the definition of phase space is identical to that used in the theory of dynamical systems; that is, an abstract space that contains all points that are necessary to describe the state of a system. For our case, the magnetization with the three orthogonal components can be described by a three-dimensional phase space. Hence, we treat the evolution of the magnetization vector subject to magnetic perturbations by examining the evolution of the vector head (point) in phase space as a function of the control parameters. As shown below, a steady state is reached when the trajectory followed by the magnetization reaches one or several fixed points. In this analysis, first we consider the establishment of steady states in the absence of phase rotation (i.e., $\beta = 0$) during each period (T_R), and later we introduce β as an additional control parameter. In SSFP imaging, T_R is typically taken to be small relative to the transverse and longitudinal relaxation constants. In other words, it is assumed that no appreciable longitudinal recovery or transverse relaxation takes place within one T_R so that thermal equilibrium is established. Throughout this analysis it is also important to bear in mind the physical limit of $T_2 \leq T_1$.

Steady-State Ensemble Magnetization when $\beta = 0$

Consider the effect of repetitive application of RF pulses that tip the ensemble magnetization about the x axis by α in the presence of spin relaxation. In the first pulse, the equilibrium magnetization \mathcal{M}_0 is rotated into a new position. The z component of the magnetization, \mathcal{M}_z , recovers longitudinally, and the transverse component \mathcal{M}_y is reduced before the next RF pulse is applied. In this setup, the other transverse component, \mathcal{M}_x , is zero and it remains zero provided $\beta = 0$. Clearly, the extent of the longitudinal recovery and transverse loss are determined by the appropriate relaxation constants. In the limit where $T_R \gg T_2$, it is clear that the tendency of the system is to reach zero magnetization. Thus, in order to have a nonzero steady-state magnetization, it is imperative that $T_R \leq T_2$. In this limit, there is always a nonzero magnetization that remains after each T_R , which is then tipped by the subsequent RF pulse. After a number of pulses, the RF tipping takes the magnetization from a point (\mathbf{r}_0) in phase space to another point (\mathbf{r}_1), and the subsequent relaxation during T_R takes it back to \mathbf{r}_0 . This condition is referred to as the steady state. Note that there are two fixed points in phase space, one prior to the pulse and one after the pulse, namely $\mathcal{M}^+(\infty)$ and $\mathcal{M}^-(\infty)$. This behavior is shown for a

select few flip angles in Fig. 1. As shown in Fig. 1(D), the greater the T_1/T_2 ratio, the greater the distance between the two fixed points.

Steady-State Ensemble Magnetization when $\beta \neq 0$

When β is nonzero, an intriguing event takes place. In this case, as β is increased, the phase trajectory moves out of the YZ plane. This is expected because the phase rotation effectively forces a nonzero \mathcal{M}_x . This leads to the establishment of two coplanar fixed points with the plane determined by β . Under these conditions, to establish steady state, the effect of RF tipping needs to be negated through relaxation *and* phase rotation over a single T_R . In the literature, it is customary to take $\mathcal{M}^+(\infty)$ as the steady-state value of the magnetization. If we adopt this convention here and follow this point in phase space for different values of β over a full period of 2π , a cyclic locus of steady-state values can be identified. This is shown in Fig. 2 for a flip angle of $\alpha = 15^\circ$.

One can relate the geometric properties of this locus to MR parameters:

1. The eccentricity of the cycle is related to T_1/T_2 ; a circle when $T_1/T_2 = 1$ and ellipse when $T_1/T_2 > 1$. This is shown in Fig. 3.
2. The plane of the locus is determined by the flip angle.
3. The points at equal intervals of β are not uniformly distributed on the locus. In particular, for any given flip angle, the points are distributed densely around $\beta = \pi$, and the exact distribution of the points on the locus is determined by the T_1/T_2 and the flip angle.
4. Because the MR signal is the orthogonal projection of the magnetization locus, it is expected that the MR signal will be dependent on the eccentricity and the plane of locus. This is shown in Fig. 4.

Geometry of the SSFP Signal on the Transverse Plane

As mentioned earlier, the transverse magnetization can be related to the geometrical properties of the orthogonal projection of the steady-state magnetization locus on the transverse plane. When $\beta = 0$, the orthogonal projection of the steady state magnetization yields a point in the transverse plane. From a dynamic sense, this state can be characterized as an unstable equilibrium, as any nonzero ΔB leads to an abrupt geometrical change that takes the point to a

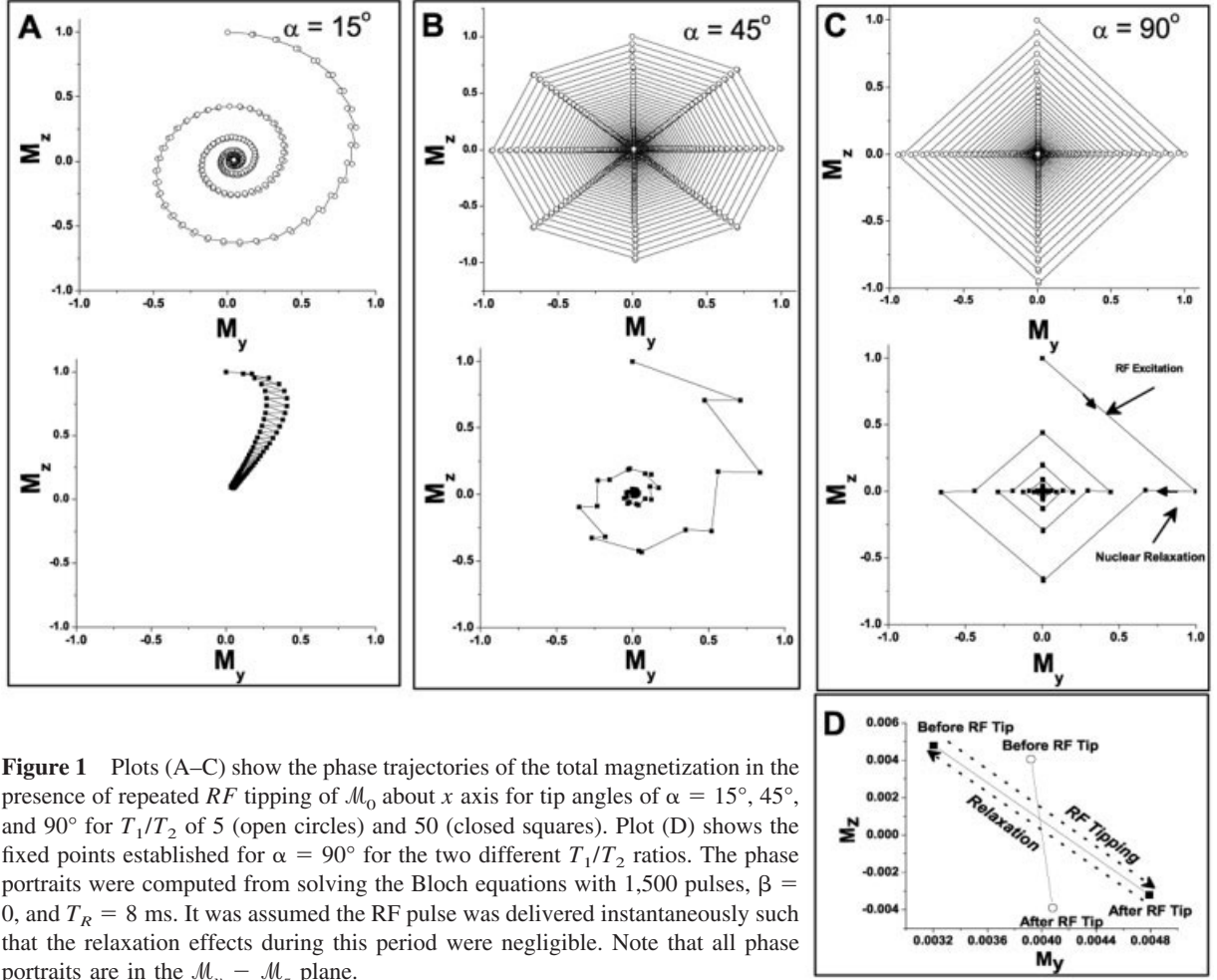


Figure 1 Plots (A–C) show the phase trajectories of the total magnetization in the presence of repeated *RF* tipping of \mathcal{M}_0 about x axis for tip angles of $\alpha = 15^\circ$, 45° , and 90° for T_1/T_2 of 5 (open circles) and 50 (closed squares). Plot (D) shows the fixed points established for $\alpha = 90^\circ$ for the two different T_1/T_2 ratios. The phase portraits were computed from solving the Bloch equations with 1,500 pulses, $\beta = 0$, and $T_R = 8$ ms. It was assumed the *RF* pulse was delivered instantaneously such that the relaxation effects during this period were negligible. Note that all phase portraits are in the $\mathcal{M}_y - \mathcal{M}_z$ plane.

locus in the transverse plane. The length of the major and minor axes and the distribution of points over the locus are determined by T_1/T_2 and α . In general, for small $T_1/T_2 \geq 1$ and small α , the locus is an ellipse with its major axis along the x axis. As T_1/T_2 or α increase, the eccentricity of the ellipse decreases and the locus becomes a circle as $\alpha \rightarrow \pi$ or $T_1/T_2 \rightarrow \infty$. More specifically, from Eqs. [19] and [20], it can be shown that the equation for the locus containing the coordinates of transverse magnetization (\mathcal{M}_x and \mathcal{M}_y) can be written as

$$\frac{\mathcal{M}_x^2}{(L_a/2)^2} + \frac{(\mathcal{M}_y + L_b/2)^2}{(L_b/2)^2} = 1, \quad [1]$$

where L_a and L_b denote the length of the major and minor axis respectively and are given by

$$L_a = \frac{2\mathcal{M}_0 \sin \alpha \sin \beta^*}{(2T_1/T_2)(1 - \cos \alpha) + (1 + \cos \alpha)(1 - \cos \beta^*)} \quad [2]$$

L_b

$$= \frac{\mathcal{M}_0 \sin(\alpha)(\cos \alpha - 1)}{(1 - T_1/T_2)\cos^2 \alpha + 2(T_1/T_2)\cos \alpha - (1 + T_1/T_2)}, \quad [3]$$

where

$$\beta^* = \cos^{-1} \left[\frac{\cos \alpha + 1}{(1 - 2T_1/T_2)\cos \alpha + 2T_1/T_2 + 1} \right]. \quad [4]$$

Refer to Appendix B for details. A contour plot showing the dependence of eccentricity, defined as

$$\text{Eccentricity}(e) = \sqrt{1 - (L_b/L_a)^2}, \quad [5]$$

on T_1/T_2 and α is shown in Fig. 5. It is also clear that the eccentricity of the locus decreases monotonically as T_1/T_2 or α increases.

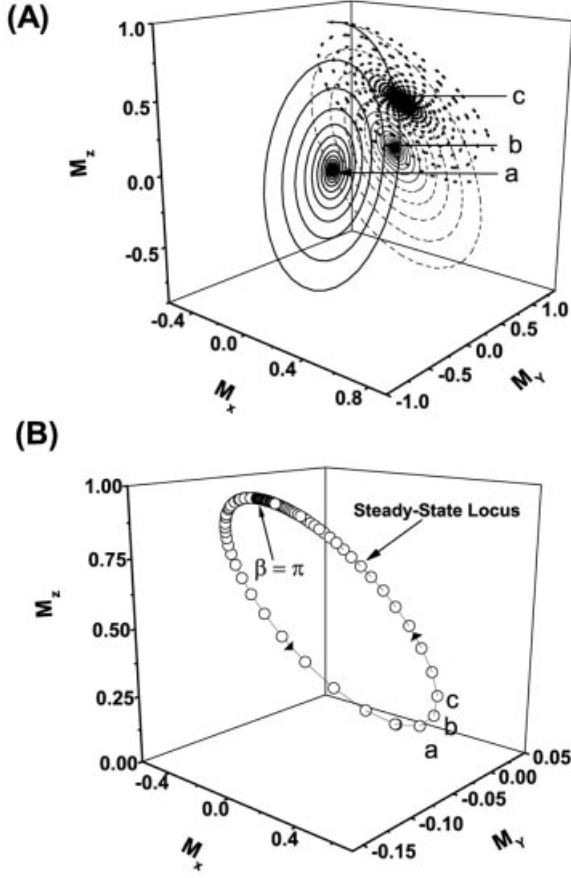


Figure 2 Plot (A) shows how the transient magnetization is modified with a nonzero β . Point a corresponds to on-resonance condition; points b and c represent off-resonance of 2 Hz and 4 Hz respectively. Note the movement of the steady-state values to different planes as β increases from a value of zero. Once a full period of β is exhausted, a locus of steady-state values is formed as shown in (B). All steady-state signal values in Fig. 2(B) were obtained with linear increments in β .

Physical Implications of the Properties of the Transverse Magnetization Locus

A. Critical Signal Values. The poles of the magnetization locus on the transverse plane, $(0, 0)$, $(\pm L_a/2, -L_b/2)$, and $(0, -L_b)$, represent points of critical signal values. That is, for all $e \in (0, 1)$, the signal attains its absolute minimum of zero at $(0, 0)$. At $e = 1$, it reaches its absolute maximum at $(\pm L_a/2, -L_b/2)$. As e decreases from 1, maximum signal values occur at different points along the ellipse. These points are symmetric about the y axis on the lower half of the ellipse and approach one another as $e \rightarrow 0$. When $e = 0$ is reached, the two symmetric points collapse into a single point at $(0, -L_b)$. The points on the upper half of the ellipse do not yield any

maxima for any $e \in (0, 1)$. In particular, it is possible to show that

$$\text{Max}\{\mathcal{M}_{xy}\} \sim \begin{cases} L_a/2 & \text{at } (\pm L_a/2, -L_b/2), & e \sim 1 \\ L_b & \text{at } (0, -L_b), & e \sim 0 \end{cases} \quad [6]$$

$$\text{Min}\{\mathcal{M}_{xy}\} = 0 \text{ at } (0, 0), \quad \text{for any } e \in (0, 1). \quad [7]$$

Refer to Appendix C for details.

B. Signal Homogeneity. The distribution of points at equal intervals of β , on the magnetization locus in transverse plane, depends on e as well. For $e \sim 1$, the points are most densely distributed around $(0, -L_b)$ and most sparsely around $(0, 0)$. Under these conditions,

$$\mathcal{M}_x \sim \text{Constant}, \quad \text{for } \beta \in \Omega \subset (0, 2\pi) \quad [8]$$

$$\mathcal{M}_y \sim -L_b, \quad [9]$$

which leads to relatively constant signal over Ω . As e decreases, this skewed distribution slowly changes and becomes uniform. As the density around $(0, -L_b)$ is lost, so does the size of Ω or the range of β over which the signal is homogeneous. When $e \sim 0$, the distribution is uniform and signal is most inhomogeneous.

From earlier discussions, it is also clear that peak signals are obtained at different points along the ellipse for a given e . When $e \sim 1$, the signal peaks around $(\pm L_a/2, -L_b/2)$ and has a dense distribution

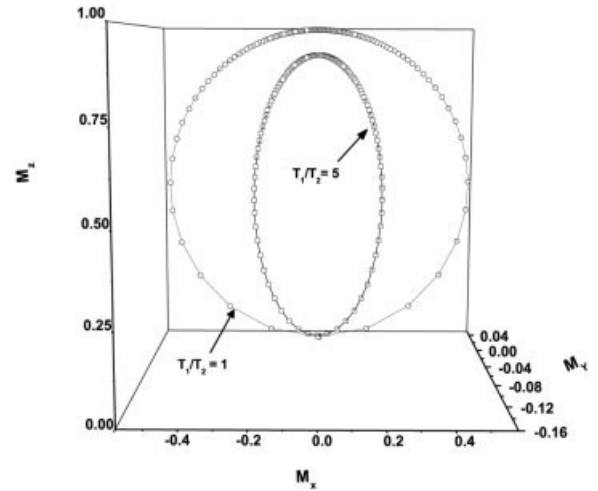


Figure 3 A plot showing the relationship between eccentricity of the steady-state locus and T_1/T_2 at $\alpha = 15^\circ$. The steady-state locus is a circle when $T_1/T_2 = 1$ and an ellipse when $T_1/T_2 = 5$. All steady-state values shown as points in steady-state loci were obtained with linear increments in β .

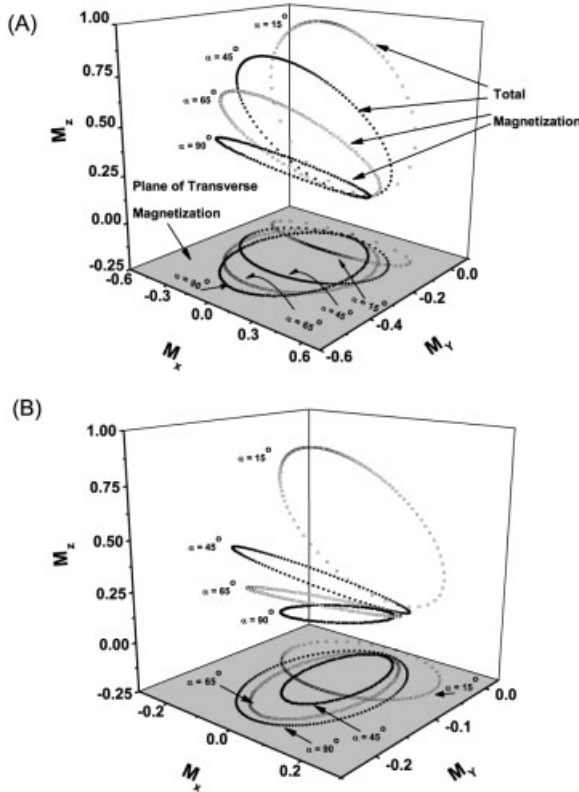


Figure 4 A plot showing that the plane of the steady-state locus is determined by the flip angle of the RF pulse and the size locus is determined by T_1/T_2 . Plot (A) and (B) show the steady-state locus for $T_1/T_2 = 1$ and 5 respectively, for various flip angles. It is clear that as T_1/T_2 or α is changed, distribution of points at equal intervals of β also changes. For smaller flip angles, increase in T_1/T_2 leads to a more uniform distribution of points, whereas with larger flip angles, the opposite happens. Note that the actual measurable MR signal is the orthogonal projection of the steady-state locus on the transverse or $M_x - M_y$ plane. All steady-state values shown as points in the steady-state loci were obtained with linear increments in β .

of points at equal intervals of β leading to uniform signal for a large Ω . However, this homogeneous signal is nearly zero, given that the points yielding such a signal have $M_x \sim 0$ and $M_y \sim L_b \sim 0$. When $e \sim 0$ is reached, the signal is fairly inhomogeneous. In practice, we want the signal to be large and homogeneous. It can be shown that this compromising condition is established when $e \sim 1/\sqrt{2}$. Thus, an optimum flip angle for an imaging application will be determined by the T_1/T_2 of the medium. One can identify the appropriate α for a given T_1/T_2 from the contour line with $e \sim 0.7$ shown in Fig. 5.

C. Signal Magnitudes. Previous discussion showed that, for a given T_1/T_2 , optimum signal values are

obtained with a proper choice of α that yields $e = 1/\sqrt{2}$. However, the discussion so far does not provide insight into the inverse problem; that is, for a given α and e , what is the effect of T_1/T_2 on the signal magnitude? As T_1/T_2 increases, the peak signal value decreases. This stems from the fact that as T_1/T_2 increases, the size of the transverse magnetization locus decreases. This leads to a concomitant reduction in the magnitudes of M_x and M_y , that maximize M_{xy} over the locus, resulting in a smaller M_{xy} .

These features are collected in a more familiar off-resonance frequency response of a spin ensemble in Fig. 6. In particular, (1) the shoulders on the off-resonance frequency response are determined by e ; (2) optimum signal, that is, signal homogeneity with relatively large signal values, for a given T_1/T_2 and α , is established when $e \sim 1/\sqrt{2}$; (3) singular peak signal around $\beta = \pi$, particularly for large α or T_1/T_2 , correspond to $e \sim 0$; (4) for any given flip angle, an increase in T_1/T_2 leads to a reduction in signal magnitude for every $\beta \in [0, 2\pi]$.

SSFP SIGNAL: FROM A SPIN ENSEMBLE TO POPULATION OF ENSEMBLES

So far we have limited our discussion to an ensemble of spins. However, in practice, an MR image is constructed with the emissions collected from a number

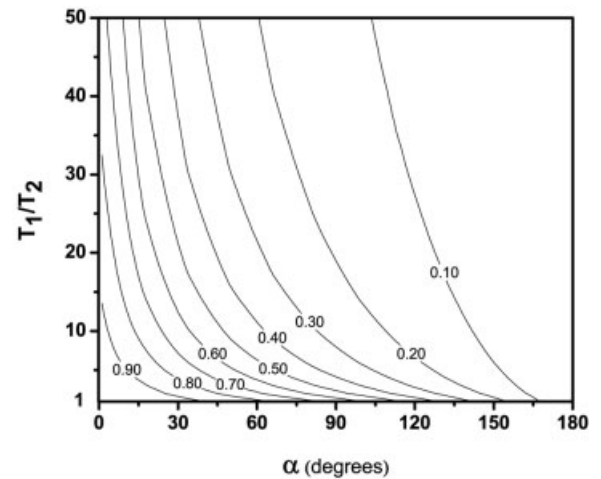


Figure 5 Contour plot showing the dependence of the eccentricity of the locus (as defined by Eq. [5]) resulting from the orthogonal projection of the steady-state locus on $M_x - M_y$ plane on T_1/T_2 and α . Equal eccentricity contours are shown with the eccentricity values on the respective curves. As T_1/T_2 or α increases, the eccentricity decreases from 1 to zero.

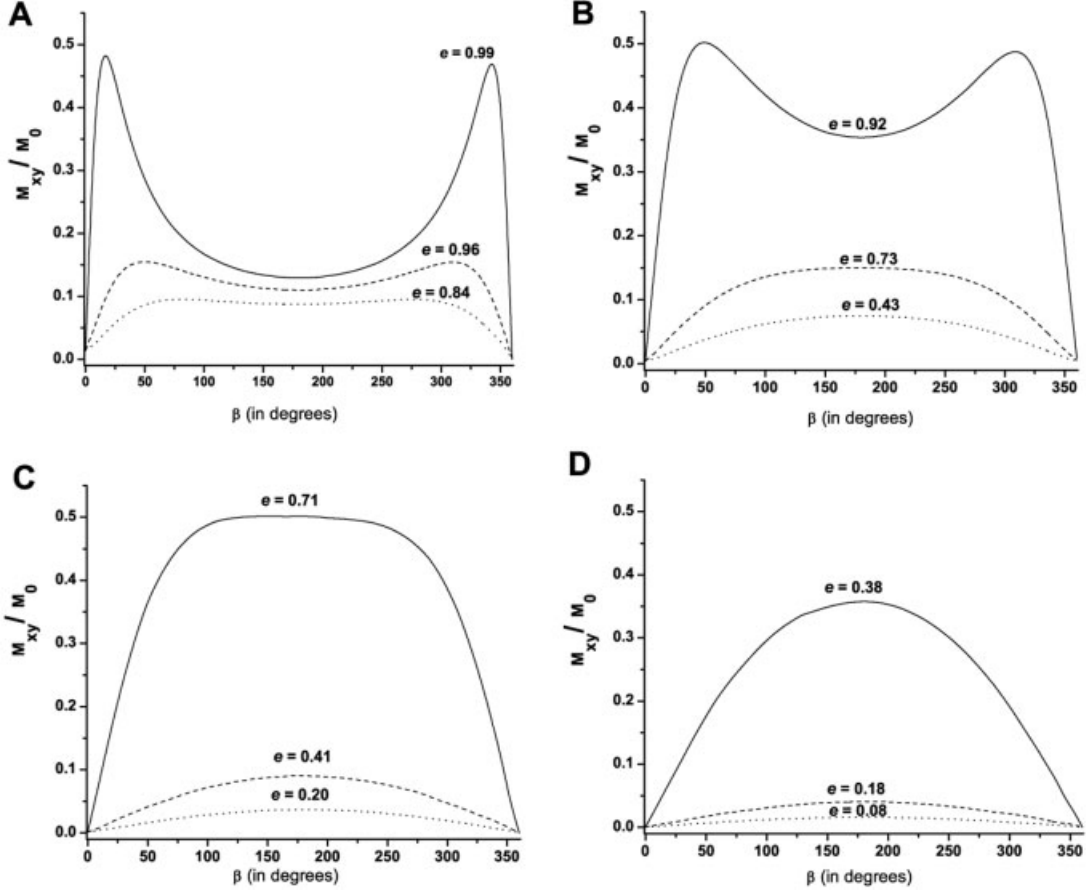


Figure 6 Plots A, B, C, and D represent the SSFP off-resonance frequency profile obtained with $T_1/T_2 = 1$ (solid lines), 5 (dashed lines), and 25 (dotted lines) for $\alpha = 15^\circ, 45^\circ, 90^\circ$, and 135° respectively. Figure also shows corresponding eccentricity (e) for the various $(T_1/T_2, \alpha)$ pairs. As discussed in text, the position and the existence of the shoulders are determined by the eccentricity (e) of the transverse magnetization locus. As e decreases from 1, the shoulders move closer and vanish when $e \sim 1/\sqrt{2}$, and singular peaks appear as e decreases further from $1/\sqrt{2}$ toward zero. It is also evident that signal is optimized (homogeneous and maximal) when $e \sim 1/\sqrt{2}$. For a given α , as T_1/T_2 is increased, the signal magnitudes also decrease for all $\beta \in [0, 2\pi]$.

of different spin ensembles. In this section we discuss the composite effect of different ensembles in establishing a bulk MR signal with the overriding goal of showing that even when different spin ensembles are considered, there are potential methods for overcoming practical problems with off resonance. For a given α and T_R , and assuming the relaxation constants are the same in the different ensembles, the transverse components of the magnetization are fully determined from Eqs. [16–21] provided one knows the value of β . Under these conditions, if β varies among the different ensembles, then the phase of the steady-state ensemble magnetization will also vary. Thus, the observed MR signal will depend on the imaging time (T_E) and will be a weighted sum of β . That is, if β is randomly distributed over an imaging volume V with a probability density of $p(\beta)$, then the total MR signal at time T_E after the RF pulse can be written as (11)

$$M(T_E) = \left| \int_V p(\beta) [\mathcal{M}_x^+(\infty; \beta) + i\mathcal{M}_y^+(\infty; \beta)] \exp(i\beta T_E/T_R) d\beta \right| \times \exp[-T_E/T_2], \quad [10]$$

where $0 < T_E < T_R$ and $\mathcal{M}_x^+(\infty) + i\mathcal{M}_y^+(\infty)$ is the complex equivalent of a two-dimensional vector with components $(\mathcal{M}_x^+(\infty), \mathcal{M}_y^+(\infty))$. If β can be biased around $\beta = \pi$, then small phase offsets from π due to field inhomogeneities can be fairly benign. A condition analogous to $\beta = \pi$ is established if the RF pulse is alternated (also known as phase cycled) about the x axis for spins on resonance ($\beta = 0$). In this setup, at steady state, the magnetization toggles between two

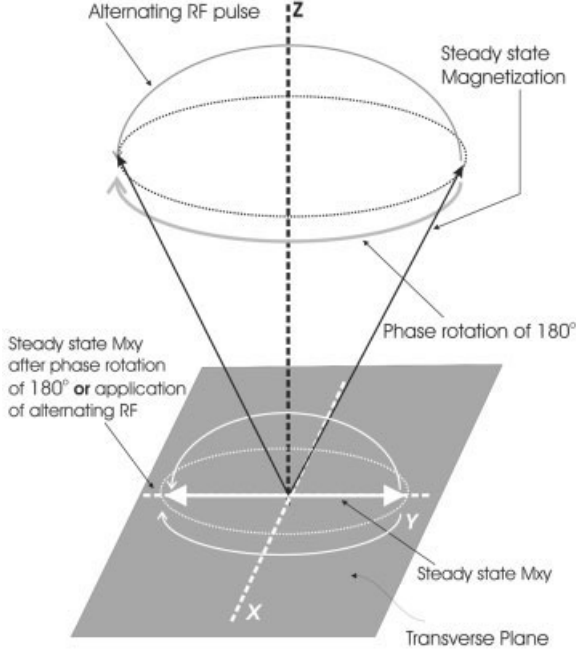


Figure 7 Plot shows the invariance of biasing the transverse magnetization around $\beta = \pi$ either with a phase rotation of π or through phase cycling for spins on-resonance.

points in the YZ plane that are symmetric about the z axis as shown in Fig. 7.

Effectively, this means that the phase rotation in the transverse plane by β becomes $\beta + \pi$. Now, if the variation in β is small so that the signal values are not disturbed (which can be done by selecting the appropriate α for a given T_1/T_2 and keeping T_R small) Eqs. [19] and [20] can be rewritten as (10)

$$\mathcal{M}_x^+ \sim 0 \quad [11]$$

$$\mathcal{M}_y^+ \sim \frac{M_0 \sin \alpha}{(T_1/T_2 + 1) - \cos \alpha (T_1/T_2 - 1)}. \quad [12]$$

Under these conditions, Eq. [10] becomes

$$M(T_E) \sim \frac{M_0 \sin \alpha}{(T_1/T_2 + 1) - \cos \alpha (T_1/T_2 - 1)} \times \exp[-T_E/T_2]. \quad [13]$$

This equation suggests that if the phase variation is small so that transverse signal homogeneity can be preserved with the appropriate choice of α and T_1/T_2 , then the spin ensembles will all behave in the same manner. If the phase rotations in the transverse plane are significantly different but still within $\pm\pi$ within a

T_R , then echoes may be observed at $T_E \leq T_R/2$ due to the refocusing effect of the phase-cycled RF pulses (11). If the phase variations are larger than $\pm\pi$, the effects of refocusing will be smaller, and signal inhomogeneity leading to image artifacts will be enhanced. For most applications, with appropriate shimming of the B_0 field, careful selection of the flip angle for a given set of relaxation time constants, keeping T_R small, and alternating the RF pulse can provide significant immunity to off-resonance effects.

SUMMARY AND CONCLUSION

In this article we demonstrated an alternate method for visualizing how SSFP signals are formed and how such signals are strongly influenced by the choice of MR parameters. In particular, we have shown that when repeated RF pulses are applied to a system that undergoes relaxation during the repetition interval, a steady state is reached and this steady state may be thought of as an unstable equilibrium with respect to off-resonance frequency. When this equilibrium is disturbed, a steady-state locus is formed in the three-dimensional magnetization phase space. We have also shown that the projection of this locus on the transverse plane represents another locus that contains the sets of all points in the off-resonance signal profile. Our analysis also showed that the major and minor axes of this locus are determined by α and T_1/T_2 . Most importantly, we showed that it is possible to understand SSFP signal properties based on the eccentricity and the size of the transverse magnetization locus.

APPENDIX A: AN ANALYTIC EQUATION FOR STEADY-STATE OF A SPIN ENSEMBLE

In the analysis to follow, “spin ensemble” refers to a collection of spins that experience an identical magnetic environment. Consider a spin ensemble with equilibrium magnetization, \mathcal{M}_0 , whose relaxation behavior is determined by the relaxation time constants T_2 and T_1 . We denote the total magnetization of this ensemble at time t by $\mathcal{M}(t) \equiv (\mathcal{M}_x(t), \mathcal{M}_y(t), \mathcal{M}_z(t))$. Now, suppose that the residual magnetization is repeatedly tipped by an RF pulse applied along the x axis rotating $\mathcal{M}(t)$ through an angle α at a set time interval, T_R . During the time between any two consecutive RF pulses (i.e., T_R), the transverse components of the magnetization (\mathcal{M}_x and \mathcal{M}_y) and the longitudinal magnetization (\mathcal{M}_z) will decay and re-

cover respectively. In addition, if a spatially invariant static field inhomogeneity (ΔB) acts on such an ensemble, then, over a given T_R , the phase of every spin within the ensemble will be advanced uniformly without altering the relaxation time constants. Note that in this analysis, we are not considering spatially varying magnetic fields that alter relaxation processes. Thus, the phase rotation of $\mathcal{M}(t)$ of a given spin ensemble in the transverse plane over every T_R can be written as $\beta = \gamma \Delta B T_R$. In addition, let the total magnetization vector immediately before and after the n^{th} RF pulse be defined by $\mathcal{M}^-(n) \equiv (\mathcal{M}_x^-(n), \mathcal{M}_y^-(n), \mathcal{M}_z^-(n))$ and $\mathcal{M}^+(n) \equiv (\mathcal{M}_x^+(n), \mathcal{M}_y^+(n), \mathcal{M}_z^+(n))$ respectively. Taking into account the relaxation behaviour of the ensemble magnetization, the effect of RF tipping, and phase rotation over a T_R , the time evolution of the total magnetization between the n and $n + 1$ RF pulses can be written as (12)

$$\mathcal{M}^-(n + 1) = R_z(\beta)S(T_R)R_x(\alpha)\mathcal{M}^-(n) + (1 - E_1)\mathcal{M}_0, \quad [14]$$

where

$$S(T_R) = \begin{bmatrix} E_2 & 0 & 0 \\ 0 & E_2 & 0 \\ 0 & 0 & E_1 \end{bmatrix}, \quad [15]$$

with $E_1 \equiv \exp(-T_R/T_1)$ and $E_2 \equiv \exp(-T_R/T_2)$; $R_z(\beta)$ and $R_x(\alpha)$ are rotation matrices representing the rotation about the z axis by angle β and rotation about the x axis by angle α respectively. At steady state, $\mathcal{M}^-(n + 1) = \mathcal{M}^-(n)$. Defining

$$\lim_{n \rightarrow \infty} \mathcal{M}^-(n) \equiv \mathcal{M}^-(\infty)$$

and

$$\lim_{n \rightarrow \infty} \mathcal{M}^+(n) \equiv \mathcal{M}^+(\infty)$$

and solving Eq. [14] gives the steady-state values (13)

$$\mathcal{M}_x^-(\infty) = \mathcal{M}_0(1 - E_1)(E_2 \sin \alpha \sin \beta)/C \quad [16]$$

$$\mathcal{M}_y^-(\infty) = \mathcal{M}_0(1 - E_1)(E_2 \sin \alpha (\cos \beta - E_2))/C \quad [17]$$

$$\mathcal{M}_z^-(\infty) = \mathcal{M}_0(1 - E_1)[(1 - E_2 \cos \beta) - E_2 \cos \alpha (\cos \beta - E_2)]/C \quad [18]$$

and

$$\mathcal{M}_x^+(\infty) = \mathcal{M}_x^-(\infty) \quad [19]$$

$$\mathcal{M}_y^+(\infty) = \mathcal{M}_0(1 - E_1) \sin \alpha (1 - E_2 \cos \beta)/C \quad [20]$$

$$\mathcal{M}_z^+(\infty) = \mathcal{M}_0(1 - E_1)[E_2(E_2 - E_2 \cos \beta) + \cos \alpha (1 - E_2 \cos \beta)]/C, \quad [21]$$

where $C \equiv (1 - E_1 \cos \alpha)(1 - E_2 \cos \beta) - E_2(E_1 - \cos \alpha)(E_2 - \cos \beta)$. Though the equations above correctly predict the quantitative behavior of SSFP signals, they offer little insight into how SSFP signals are formed. In the next section we provide a geometric description of SSFP signal formation that provides an intuitive understanding of SSFP signals.

APPENDIX B: EQUATIONS FOR L_a AND L_b

To find the critical points of \mathcal{M}_x in the domain of β we set the derivative of Eq. [16] with respect to β to zero. This yields

$$\cos \beta = \frac{E_2(1 - E_1 - E_1 \cos \alpha + \cos \alpha)}{1 - E_1 \cos \alpha - E_2^2(E_1 - \cos \alpha)}. \quad [22]$$

Applying the approximations, T_R/T_1 and $T_R/T_2 \ll 1$, and retaining only the leading order terms gives

$$\cos \beta = \frac{1 + \cos \alpha}{(1 - 2(T_1/T_2)) \cos \alpha + 2(T_1/T_2) + 1}. \quad [23]$$

In the interval $\beta \in [0, 2\pi]$, there are two values solutions for the Eq. [23], namely β^* and $2\pi - \beta^*$, where β^* is given by Eq. [4]. Applying the extreme value theorem ensures that these critical values correspond to absolute maximum and minimum values of \mathcal{M}_x . A similar analysis using \mathcal{M}_y identifies the absolute maximum and minimum of \mathcal{M}_y at $\beta = 0$ and π . Using these critical values of \mathcal{M}_x and \mathcal{M}_y , the characteristic lengths of the locus can be determined. That is,

$$L_a = |\mathcal{M}_x(\beta^*) - \mathcal{M}_x(2\pi - \beta^*)| \quad [24]$$

$$= 2\mathcal{M}_x(\beta^*) \quad [25]$$

$$= \frac{2\mathcal{M}_0 \sin \alpha \sin \beta^*}{(1 - E_1 \cos \alpha)(1 - E_2 \cos \beta) - E_2(E_1 - \cos \alpha)(E_2 - \cos \beta)}. \quad [26]$$

Applying the approximations, T_R/T_1 and $T_R/T_2 \ll 1$, and retaining only the leading order terms gives

Eq. [2]. A similar analysis using Eq. [17] using the critical points gives Eq. [3]. From here it can be shown that $L_a > L_b$ for $T_1/T_2 \in (1, \infty)$ and $\alpha \in [0, \pi]$, which identifies L_a as the major axis and L_b as the minor axis of the magnetization locus in the transverse plane.

APPENDIX C: MAXIMUM SSFP SIGNALS ON MAGNETIZATION LOCUS FOR $E = 0$ OR 1

To determine the maximum signal values at the extremes values of e , that is at $e = 0$ and 1, we combine the signal equation $\mathcal{M}_{xy}^2 = \mathcal{M}_x^2 + \mathcal{M}_y^2$ with Eq. [1]. This yields

$$\left(\frac{\mathcal{M}_{xy}}{(L_d/2)}\right)^2 = 2(1 - (L_d/L_b)^2)(\mathcal{M}_y/(L_b/2))^2 + 2(L_d/L_b)^2(\mathcal{M}_y/(L_b/2)), \quad [27]$$

which can be written as

$$f(y)^2 = 2(1 - a^2)y - 2a^2, \quad y \in [-2, 0]. \quad [28]$$

To find the maximum value of f when $e = 1$, we apply the first derivative test and take $a \gg 1$. This shows that f is maximum when $y = -1$ or the SSFP signal has a maximum value of $L_d/2$ at $(\mathcal{M}_x, \mathcal{M}_y) = (\pm L_d/2, -L_b/2)$. To find the absolute maximum when $e = 0$, we set $a = 1$ in Eq. [1], which gives

$$f^2 = -2a^2y. \quad [29]$$

On $y \in [-2, 0]$, f has a maximum when $y = -2$. This implies that the maximum signal value of L_b occurs at $(\mathcal{M}_x, \mathcal{M}_y) = (0, -L_b)$.

REFERENCES

1. Carr H. 1958. Steady-state free precession in nuclear magnetic resonance. *Phys Rev* 112:1693–1701.
2. Oppelt A, Graumann R, Barfub H, Fischer H, Hartl W, Schajor W. 1986. FISP—a new fast MRI sequence. *Electromedica* 54(1):15–18.
3. Hawkes RC, Patz S. 1987. Rapid Fourier imaging using steady-state free precession. *Magn Reson Med* 4:9–23.
4. Foo TK, Ho VB, Marcos HB, Hood MN, Choyke PL. 2002. MR angiography using steady-state free precession. *Magn Reson Med* 48:699–706.

5. Scheffler K. 2001. T_1 quantification with inversion recovery TrueFISP. *Magn Reson Med* 45:720–723.
6. Deoni SC, Ward HA, Peters TM, Rutt BK. 2004. Rapid T_2 estimation with phase-cycled variable nutation steady-state free precession. *Magn Reson Med* 52:435–439.
7. Scheffler K. 2004. Fast frequency mapping with balanced SSFP: theory and application to proton-resonance frequency shift thermometry. *Magn Reson Med* 51:1205–1211.
8. Dharmakumar R, Hong J, Brittain JH, Plewes DB, Wright GA. 2005. Oxygen-sensitive contrast in blood for steady-state free precession imaging. *Magn Reson Med* 53:574–583.
9. Scheffler K. 1999. A pictorial description of steady-states in rapid magnetic resonance imaging. *Concepts Magn Reson* 11(5):291–304.
10. Roberts JD. 1991. The Bloch equations. How to have fun calculating what happens in NMR experiments with a personal computer. *Concepts Magn Reson* 3(1):27–45.
11. Scheffler K, Hennig J. 2003. Is TrueFISP a gradient-echo or a spin-echo sequence. *Magn Reson Med* 49:395–397.
12. Haacke EM, Brown RW, Thompson MR, Venkatesan R. 1999. *Magnetic resonance imaging: physical principles and sequence design*. New York: John Wiley & Sons 451–512.
13. Sekihara K. 1987. Steady-state magnetizations in rapid NMR imaging using small flip angles and short repetition intervals. *IEEE Trans Med Imaging* MI-6(12):157–164.

BIOGRAPHIES



Rohan Dharmakumar completed his bachelor of science in theoretical physiology and physics, master of science in mathematics, and Ph.D. in medical physics in 2004 from the University of Toronto, Canada. He is currently a postdoctoral fellow at the University of Toronto. His research interests include cardiovascular magnetic resonance imaging, spin physics, and contrast-enhanced

MRI.



Graham Wright completed his Ph.D. at Stanford in 1991 on oxygen-sensitive MRI. Since 1993 he has been at the University of Toronto where he is now a professor in the Department of Medical Biophysics and Director of the Heart and Circulation Research Program at Sunnybrook & Women's College Health Science Centre. His research focus is cardiovascular MRI, where he has published more than 50 papers and holds 10 patents.